Quantum Efficiency and Optical Cross-talk of Pixels with Backside Scattering Technique for Near-Infrared Imaging

Tae-Yon Lee, Seungjae Oh, Taehyoung Kim, Hongki Kim, Jihyun Kwak, Masaru Ishii, Surim Lee, Hyoju Kim, Yoonjay Han, Changhwa Kim, Jaehoon Jeon, Dongseok Cho, Seung Sik Kim, Jonghyun Go, In-Gyu Baek, Hyuksoon Choi, Jaekyu Lee, and Chang-Rok Moon

Semiconductor R&D Center, Samsung Electronics Co.,Ltd.,
Samsungjeonja-ro 1, Hwaseong-si, Gyeonggi-do 18448, Korea,
telephone: +82-31-325-3061, email: taeyon.lee@samsung.com

Abstract-We present performance of image sensor pixel with the structure of surface-limited local trench array to achieve backside scattering technique (BST), to enhance quantum efficiency of CMOS image sensor, especially at near-infrared wavelength. The pixel with BST structure of selection is demonstrated to exhibit significant improvement of quantum efficiency at 940nm, 1.5 times higher than that of pixel without BST, with acceptable inter-pixel cross-talk.

I. Introduction

The need of CMOS image sensor (CIS) with elevated quantum efficiency (QE) at near infrared (NIR) wavelength is growing rapidly. To enhance NIR QE, it is essential to increase the optical path length and scattering probability inside the pixel, hence the use of thick Si epi-layer as well as modification of photodiode surface to achieve backside scattering technique (BST) are viable options [1]. Following our continuing efforts to maximize the performance and functions of our global shutter pixel sensor [2], we have investigated optical characteristics of pixels with BST for NIR imaging as presented in this study. We used pixel and process of full-depth front-side deep trench isolation (FDTI) together with vertical transfer gate [3], preferable for the formation of thick photodiode, as the reference architecture of comparison.

II. Fabrication and Experimental

A 1/5-inch stacked sensor with 1.0Mpixel array of 2.3 μm pixel is fabricated using standard 28 nm logic- and 1-poly 6-metal 65 nm (FEOL) / 45 nm (BEOL) pixel- processes for CIS, with a process flow as in Figure 1. Wafers of logic, and FDTI pixel array are prepared separately as in Fig.1 (a). The pixel- and logic- wafers are bonded as in Fig.1 (b): Electrical contact between pixel- and logic-wafers is made by Cu-Cu contact by inter-wafer via (not shown). After proper epi-Si thinning process,

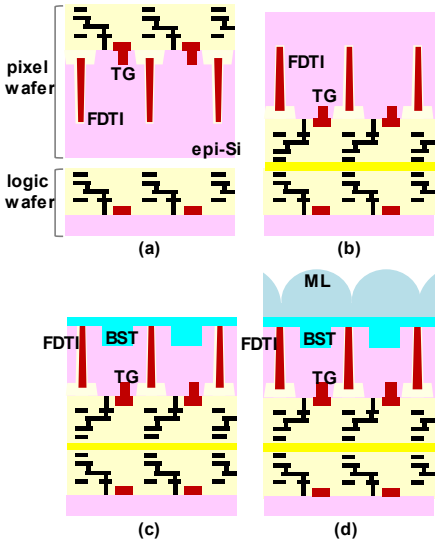

Figure 1. Fabrication flow of pixel array containing BST. The ARL, metal layers, and inter-layer dielectrics are marked with sky-blue, black, and light-yellow, respectively.

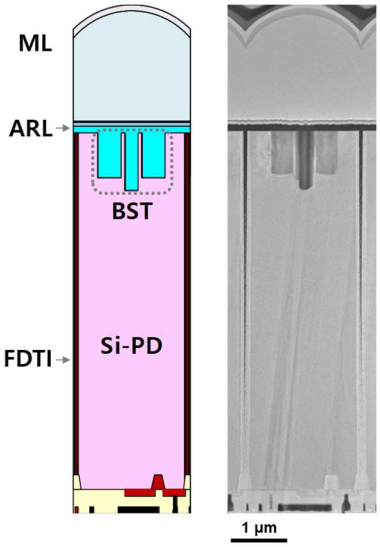

Figure 2. Vertical schematic of 2.3μm FDTI pixel containing BST (left), reproduced after full integration (right).

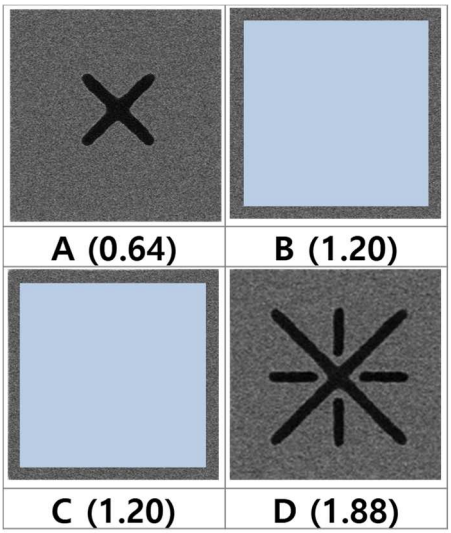

Figure 3. Plan view SEM images obtained after formation of BST before ARL filling, at the step of Fig.1 (c). Normalized BST area is given in the parenthesis. Details of B- and C- shape BST structures are not given.

BST structures, a few μm deep surface-limited trench is etched, followed by filling with anti-flection layer (ARL) providing optimal optical transmittance as well as suppressing dark current, on the Si-photodiode surface as in Fig. 1 (c). Deposition of planarization layer and formation of micro-lens (ML) array follow as in Fig.1 (d), lastly.
Figure 2 shows cross sectional TEM photograph of pixel with BST after full fabrication. All the pixel constituents, including deep photodiode with FDTI filled with isolating oxide and doped poly Si, as well as BST, are well reproduced as designed.
Figure 3 shows plan-view SEM image of several BST structures after etching Si surface without ARL filling at the step of Fig.1 (c). Among various BST structures, performance of selected geometries is discussed in this study.

III. Results and Discussion

Figure 4 shows vertical profile of optical intensity obtained from Finite-Difference Time-Domain (FDTD) simulation. In contrast to pixel without BST, pixel with BST exhibits wide-spread light scattering, which increases effective optical path length and improves QE_{940nm} eventually. From FDTD simulation comparison, especially between B- and C- shape BST pixels, we confirmed that each BST pixel exhibits its own degree of light intensity localization around BST and propagation to FDTI: Unique photon absorption properties of each pixel evolve and result in different QE_{940nm} in combination, not just dependent on BST volume.

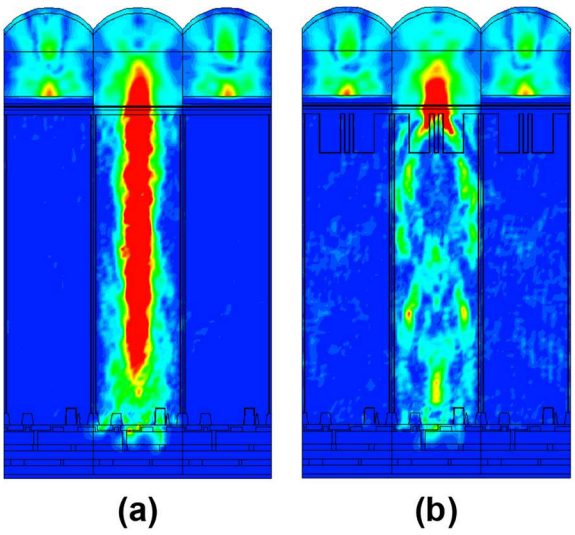

Figure 4. Light power profile, without (a) and with (b) D-shape BST calculated from FDTD simulation for 940nm wavelength light. To check light propagation into neighboring pixels, light incidence into periphery pixels are blocked.

Figure 5 shows a typical example of spectral QE, comparing between pixels with- and without- BST: Over the whole range of wavelengths, pixel with BST shows higher QEs than those of pixel without BST, except in visible wavelength from 550 nm to 650 nm in which the two pixel shows similar QE. This feature is observed with the all the pixels of BST structures shown in Fig.3.
Figure 6 summarizes relation between QE_{940nm} and BST surface area of selected BST structures of Fig.3. Significant QE_{940nm} improvement of pixels with BST is noticed, and QE_{940nm} of C-shape BST pixel is 1.49 times higher than that of pixel without

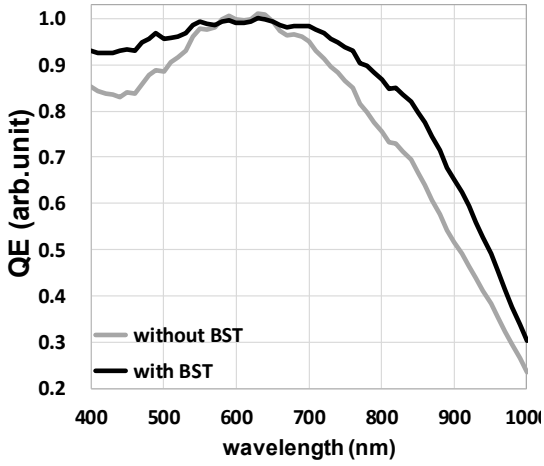

Figure 5. Comparison of spectral QE between pixel with- and without- BST. Result of D-shape BST but different depth from pixels in Fig.3 is presented.

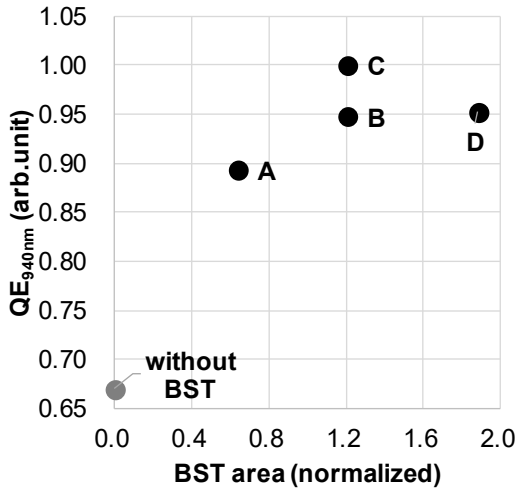

Figure 6. Dependence of QE_{940nm} on the area of BST structure. For comparison, QE_{940nm} of pixel without BST is given with gray circle.

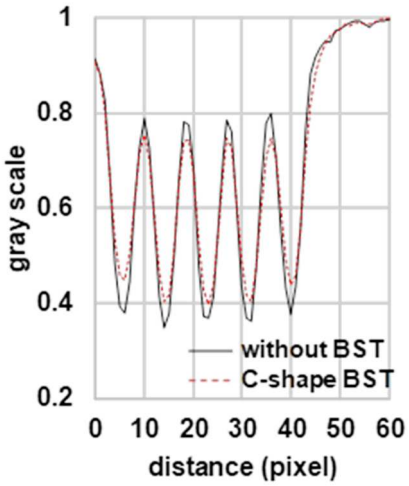

Figure 8. Signal amplitude profiles from dotted area of yellow regions in Figs.7 (a) and (b).

BST. It is noticed that QE_{940nm} does not show monotonic dependence on BST volume, as expected from FDTD simulation; D-shape BST pixel exhibits less QE_{940nm} than C-shape BST pixel; QE_{940nm} of C-shape BST pixel is 1.05 times higher than that of B-shape BST pixel with all the same BST geometry and volume.

From the FDTD simulation in Fig.4, it is expected that the scattered light, above critical angle of incidence especially for BST pixels, can penetrate to neighboring pixel to cause optical cross-talk. For quantitative analysis, images of international-standard-organization (ISO) test chart are captured by sensor with imaging lens of F#2.8 and 940 nm band pass filter under illumination of 3200K light source as in Figure 7. Every fine feature of test chart is well resolved for both sensors; The zoomed-in image (red dotted box) from sensor with C-shape BST in Fig. 7 (b) shows degraded contrast in comparison to Fig.7 (a). More quantitatively, the signal profile in the yellow dotted box in Figs. 7 is compared in Figure 8. It is clear that the signal contrast of C-shape BST pixel sensor, 27.2%, is smaller than 36.4% from sensor of pixel without BST.

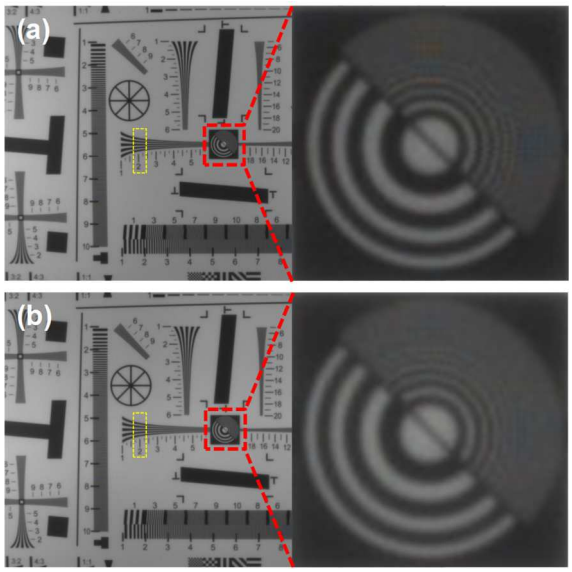

Figure 7. ISO standard test chart images captured by sensors (a) without and (b) with C-shape BST. Images were taken with imaging lens of F#2.8 and 940 nm band pass filter under 3200K illumination.

Characterization of sensor modulation-transfer-function at the half of Nyquist frequency (MTF_{940nm}) with slanted-edge method [3] is carried out from images of Figs. 7, and Figure 9 shows relation between the amplitude of MTF_{940nm} and the area of BST structure. It is shown that pixels with BST show poor MTF_{940nm} in comparison to pixel without BST; the BST pixel with improved QE_{940nm} shows degraded MTF_{940nm}, in general. It can be interpreted that increased optical path length makes the penetration of photon to the neighboring pixel more probable to degrade MTF performance, not only to enhance QE.

Structural modifications of the pixel along with BST geometry can reduce the optical cross-talk without QE_{940nm} drop. One of methods can be the use of thicker isolation oxide in FDTI; D'-shape BST pixel, with isolation oxide two times thicker than that of D-shape BST pixel, shows MTF_{940nm} of significant improvement, in comparison to 0.81 of D-shape BST pixel, as in Fig. 9. Thicker oxide is interpreted to hinder light scattering to neighboring

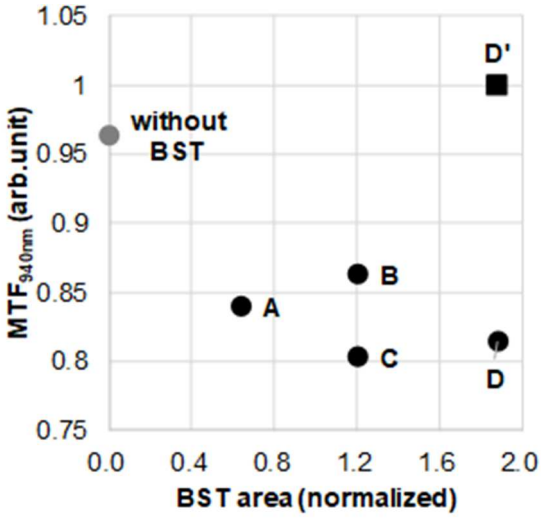

Figure 9. Correlation check between sensor MTF_{940nm} and the surface area of BST structure. The sensor MTF_{940nm} is obtained from 108 line-pair/mm (half of the Nyquist frequency of 2.3 μm pixel pitch sensor), divided by lens MTF_{940nm} measured independently. For comparison, results of pixel without BST structure (gray circle) as well as D'-BST pixel of FDTI structure modification from D-BST (black square) are provided.

pixel, in effect.

IV. SUMMARY AND CONCLUSION

The BST is demonstrated to enhance NIR QE with an acceptable inter-pixel optical cross-talk, for FDTI pixel of thick photodiode. We found that selection of C-shape BST allows better performance advantages compared to the other BST structures. Comparison of QE_{940nm}, MTF_{940nm}, and dark current between pixel without BST and C-shape BST pixel is summarized in Table 1. In combination with thick Si epi-layer, the use of C-shape BST is shown to boost NIR QE significantly. At present, dark current of pixel with BST is poorer than the pixel without BST. The degradation is still acceptable for application in NIR imaging, typically under use of active light source. While for application in more extended areas, dark current improvement of pixel with BST is favorable. With optimal ARL structure and process [5], dark current degradation due to formation of BST structure can be suppressed, and on-going research efforts are in progress.

	No BST	C-shape BST
QE_{940nm} (arb.unit)	0.67	1.00
MTF_{940nm} (arb.unit)	1.0	0.83
Dark Current (arb.unit)	1.0	1.1

Table 1. Comparison of QE_{940nm} , MTF_{940nm}, and dark current among sensors of C-BST pixel and pixel without BST.

REFERENCES

[1] J. Park *et al.*, "Pixel Technology for Improving IR Quantum Efficiency of Backside-illuminated CMOS Image Sensor", *Proc. International Image Sensor Workshop*, R14 (2019).

[2] J.K. Lee *et al.*, "A 2.1 e- Temporal Noise and -105 dB Parasitic Light Sensitivity Backside-Illuminated 2.3μm Pixel Voltage-Domain Global Shutter CMOS Image Sensor Using High-Capacity DRAM Capacitor Technology", *2020 ISSCC Dig. Tech. Pap. I.*, pp.102-103 (2020).

[3] J.C. Ahn *et al.*, "A 1/4-inch 8Mpixel CMOS Image Sensor with 3D Backside-Illuminated 1.12μm Pixel with Front-Side Deep-Trench Isolation and Vertical Transfer Gate", 2014 ISSCC Dig. Tech. Pap., pp.124-125 (2014).

[4] X. Xie *et al.*, "Regularized Slanted-Edge Method for Measuring the Modulation Transfer Function of Imaging Systems", *Appl. Optics*, vol. 57, pp.6552-6558 (2018)

[5] R. Fontaine *et al.*, "A Survey of Enabling Technologies in Successful Consumer Digital Imaging Products", *Proc. International Image Sensor Workshop*, R06 (2017).